ORIGINAL PAPER

Effect of land use land cover changes on land surface temperature during 1984–2020: a case study of Baghdad city using landsat image

Bassim Mohammed Hashim[1] · Ali Al Maliki[1] · Maitham A. Sultan[1] ·
Shamsuddin Shahid[2] · Zaher Mundher Yaseen[3,4,5]

Abstract

Urban land surface temperature (LST) is dependent on many factors, including land cover, building materials, urban density, and other human activities. The current study evaluated Baghdad's LST and urban heat island (UHI) changes during 1984–2020, one of the world's hottest capital cities. The study also examined the relationship between LST and various land use and land covers (LULC). The Landsat data (TM and OLI/TIRS) data were used to retrieve normalized difference vegetation index (NDVI) and normalized difference built-up index (NDBI). Results showed increases in LST in Baghdad between 1984 and 2020 due to increased urbanization, decreased green lands, and expansion of baren areas. The highest LST is associated with residential and barren areas, ranging from 46.7 to 52.7 °C, while lowest with water bodies and orchards areas, ranging between 25 and 30.4 °C. UHI effect appeared clearly in 2020 in different parts, particularly in suburban areas around Baghdad. Higher LST was observed in less vegetated areas and vice versa. The study revealed that the average maximum temperature in Baghdad increased from 40.2 °C in 1984 to 47 °C in 2020 or about 6.8 °C during 36 years. The NDVI showed a negative correlation and NDBI a positive correlation with LST. The results improved the understanding of urban LST's relation to LULC in developing an inclusive climate resilience policy and making Baghdad more sustainable to face the consequences of climate change.

Keywords Climate change · Land surface temperature · Urban heat island · Landsat images

✉ Zaher Mundher Yaseen
zaheryaseen88@gmail.com

1   Environment and water Directorate, Ministry of Science and Technology, Baghdad, Iraq

2   School of Civil Engineering, Faculty of Engineering, Universiti Teknologi Malaysia (UTM),
     81310 Johor Bahru, Malaysia

3   Department of Urban Planning, Engineering Networks and Systems, Institute of Architecture
     and Construction, South Ural State University, 76, Lenin Prospect, 454080 Chelyabinsk, Russia

4   New Era and Development in Civil Engineering Research Group, Scientific Research Center, Al-
     Ayen University, Thi-Qar 64001, Iraq

5   College of Creative Design, Asia University, Taichung City, Taiwan

1 Introduction

Increased urbanization and global climate change are the leading cause of increasing urban land surface temperature (LST) (Sun et al. 2013). There has been an increase in urban LST due to the continuous increase in the built-up environment in most major cities world-wide (Hussain et al. 2014; Fan et al. 2017). More than 50% of the global population lives in cities, which would reach up to 66% by 2050 (Ayanlade 2016). The extensive urban growth has challenged the pursuit of sustainable and prosperous cities globally (Sanikhani et al. 2018; Kemarau and Eboy 2020; Pour et al. 2020). The change in land use land cover (LULC) leads to loss of agricultural lands and forest cover, an increase in barren areas, and impermeable surface cover because of the built-up area (Kumar et al. 2012; Fu and Weng 2016; AL-Shammari et al. 2021; Uddin et al. 2021).

The LST of an area is governed by various physical factors, i.e., topography, land use and vegetation, of the city/urban areas (Khan et al. 2021). Besides, the distribution of vegetation, built-up, open land, water bodies and other features determine the surface temperature (Chen et al. 2006). One of the widely recorded and evident impacts of urbanization is the increased temperature over the cities relative to the adjacent rural areas or the urban heat island (UHI) (Tran et al. 2006; Calice et al. 2017). UHI occurs due to land cover transformations, mainly replacing natural vegetation and agricultural lands with impervious surfaces, such as concrete, asphalt, rooftops and building walls (Buyantuyev and Wu 2009). Besides, different factors determine the extent of UHI, such as LULC, seasonal variations, ecological context, city structure, city size, urban geometry, and study area location (Lo and Quattrochi 2003; Singh et al. 2014). However, LST is mainly controlled by LULC (Kumar and Shekhar 2015). Some of the LULC, such as vegetation, is linked to the biophysical characteristics of the plants and affects the spatial patterns of surface energy, providing cooling and humidifying effects on the surrounding environments (Feng et al. 2018). The changes in LCLU and increase in the built-up area contribute to the rise of UHI, leading to the deterioration of the urban ecological and environmental quality (Mallick et al. 2013; Bao et al. 2016).

The urban sprawl due to increased demands for land for housing, industry and infrastructure cause the transformation of more agricultural land at the edges of cities (Wadduwage et al. 2017). The principle of urban–rural gradients was initially proposed to delineate the features of urbanization (McDonnell and Pickett 1990). These characteristics primarily involve land cover structures, the biota of the urban–rural area and socioeconomic dimensions (Hahs and McDonnell 2006). Urban expansion in the cities of developing countries is often discrete and inconsistent with the local plans and policies. For example, Baghdad, the capital of Iraqi, is a fast-growing urban area, accompanied by rapid unplanned changes in LULC, which affected the city's local climate (http://www.unhabitat.org/). Baghdad suffers worsening housing crisis mainly due to rapid population growth and internal migration, which led to random housing (Qeisi 2012). Another problem is the high-density traffic in Baghdad, which negatively impacts the city's environment through air pollution (Jassim et al. 2014).

One of the effective ways of retrieving regional and global LST is the remote sensing technique (Tran et al. 2006; Prakash and Norouzi 2020). Landsat TM, ETM + and OLI/TIRS have been widely used for retrieving LST at local, regional and global scales. This is because of their relative high resolution (Stathopoulou and Cartalis 2007; Cai et al. 2011), compared to other remote sensing sensors like MODIS and AVHRR. Many studies have used Landsat images to estimate LST and UHI and determine the LULC changes (e.g.,

(Sekertekin, Kutoglu, and Kaya; Lv and Zhou 2011; Rahman et al. 2012; Fu and Weng 2016; Faqe Ibrahim 2017). There are also contemporary real-life case studies of UHI using remote sensing techniques (Beyaztas et al. 2019; Faroughi et al. 2020; Terfa et al. 2020; Karimi Firozjaei et al. 2021).

In this study, the main objectives are (i) to employ multi-temporal Landsat images to calculate the LST of Baghdad and determine the UHI effects (Landsat 5 TM data for 1984, and Landsat 8 OLI data for 2020); (ii) to determine the relationship between different categories of LULC and LST; (iii) to identify the effects of LULC changes on the LST between 1984 and 2020; and (iv) to determine the impact of climate changes on temperature, UHI and LST in Baghdad from 1984 to 2020; and (v) to analyze urban–rural gradient of Baghdad City.

2 Materials and methods

2.1 Study area

Iraq is located in the Middle Eastern region bordered by Iran in the east, Syria and Turkey to the north, Saudi Arabia, Jordan, and Kuwait to the south and the Gulf to the southeast (Yaseen et al. 2019). Baghdad, the capital of Iraq, is located in the middle of Iraq and positioned on longitudes 44° 10′, 44° 33′ E and latitudes 33° 10′, 33° 27′ N, as shown in Fig. 1.
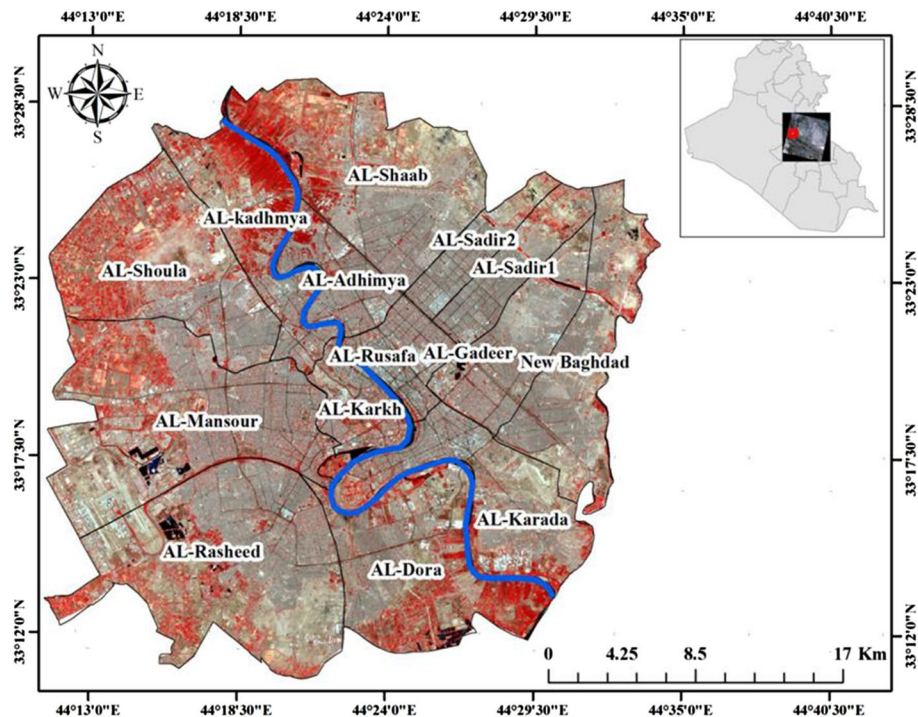

Fig. 1 Location of Baghdad in Iraq

The climate of Iraq region is varied from the north, middle and the south (Oleiwi et al. 2018). Currently, Iraq has about 40 million and close to 70% of the people in Iraq live in the cities. Nearly 8.34 million of 20% of the Iraqi population lives in Baghdad (Sarsam and Khafaji 2019). Iraq region has experienced much attention over the last decade on diverse aspects of climate and hydrology and more efforts are needed for the better understanding of the climate influence over the past few decades (Salih et al. 2020; Salman et al. 2021). Baghdad municipality has 14 administrative units, with 8 in Rusafa and 6 in Karkh, totaling about 900 km^2. This area has a hot desert climate, characterized by extreme temperatures, low relative humidity, little precipitation, and high solar radiation (Hashim et al. 2020).

2.2 Available data

This study relied on the satellite images for Baghdad city, acquired during the dry season (August) with clear atmospheric conditions using Landsat 5 TM and Landsat 8 OLI. The images were downloaded from the United States Geological Survey (www.earthexplorer. usgs.gov). The first Landsat 5 TM image was acquired on August 27 1984, while the second Landsat 8 OLI image was acquired on August 30, 2020. The images were corrected geometrically and radiometrically to enhance the image quality. The thermal bands used in this study were band 6 of Landsat 5 and bands 10 and 11 of Landsat 8. The multispectral bands of the Landsat 5 TM and Landsat 8 OLI data have 30 m spatial resolution, while the thermal band 6 of Landsat5 TM and thermal bands 10 and 11 of Landsat8 TIRS have 120 m and 100 m spatial resolution, respectively. These images were resampled to 30 m resolution to comply with Landsat 8 images. Thermal bands data in the Landsat series provide important information about soil moisture and heat units in urban areas and are particularly useful for tracking how land is being used (https://www.usgs.gov/faqs/what-are-band-designations-landsat-satellites).

Table 1 presents the features of each satellite and the bands used for LST estimation (Masek et al. 2020). The Iraqi Meteorological Organization and Seismology (IMOAS) provided Baghdad's monthly maximum average temperature data for August 1984 and 2020, which were used for validation (http://meteoseism.gov.iq/). The availability of high-resolution data combined with GIS and statistical models can provide a range of alternative approaches to defining rural and urban areas (Gajić et al. 2021).

2.3 Methodology

For monitoring LULC change and LST calculation, it is necessary to have at least the data of two periods. The remote sensing approach usually involves the usage of two or multiple dates for quantifying the land use and land cover changes in any area (Alam et al. 2020). The LULC information can be obtained from the multiband raster imageries through image interpretation and classification (Li et al. 2014). The study deals with the different processes for analyzing Landsat images: (1) Landsat images classification; (2) NDVI and NDBI calculation; (3) LST calculation for Landsat 5 TM and Landsat 8 OLI images; (3) ArcGIS 10.4.1 used to perform all processes of Landsat images and NDVI, NDBI analysis, therefore, the methodology of current study as shown in Fig. 2.

Table 1 The characteristics of Landsat 5 TM and Landsat 8 OLI (Masek et al. 2020)

Details of Landsat 5 TM Satellite Images

Band Number	Spectral Range (μ m)	Spatial Resolution (m)	Band Name
1	0.45–0.52	30	Blue
2	0.525–0.605	30	Green
3	0.63-.069	30	Red
4	0.76–0.90	30	NIR
5	1.55–1.75	30	MIR
6	10.40–12.5	120	Thermal
7	2.080–2.35	30	MIR

Details of Landsat 8 OLI Satellite Images

Band Number	Spectral Range (μ m)	Spatial Resolution (m)	Band Name
1	0.43–0.45	30	Coastal/Aerosol
2	0.45–0.51	30	Blue
3	0.53–0.59	30	Green
4	0.63–0.67	30	Red
5	0.85–0.87	30	NIR
6	1.56–1.65	30	SWIR1
7	2.10–2.29	30	SWIR2
8	0.50–0.67	15	Pan
9	1.36–1.38	30	Cirrus
10	10.60–11.19	100	TIR1
11	11.50–12.51	100	TIR2

2.3.1 Landsat images classification

The supervised classification of the Landsat images for Baghdad during 1984–2020 was used to assess how LULC changed during the study period. Besides, it was used to assess the influence of different LULC on LST. Landsat TM and OLI images were verified for geometric accuracy, and all images were processed using ArcGIS 10.4.1. These multispectral images were atmospherically and geometrically corrected in the course of pre-processing. The images were analyzed according to their spectral and spatial profiles. The statistical characteristics of the land cover categories were developed once the training sites were digitized. Many methods are being used to implement the supervised classification, such as parallelepiped classification, K-nearest neighbor, and minimum distance classification (Zhu et al. 2006). The maximum likelihood algorithm quantitatively evaluates both the variance and covariance of the spectral response patterns, and each pixel is assigned to the class for which it has the highest association (Shalaby and Tateishi 2007). The maximum likelihood algorithm was applied to classify the study area into seven classes: water, green lands, agriculture, streets, grass areas, residential areas and barren areas, as shown in Table 2. Classification accuracy assessment is very important in land use mapping and understanding map quality and reliability (Erasu 2017). With the development of the error-matrix important accuracy assessment elements, such as overall accuracy, omission error, commission error, and kappa coefficient, can be obtained (Lu and Weng 2007). The two classified maps were
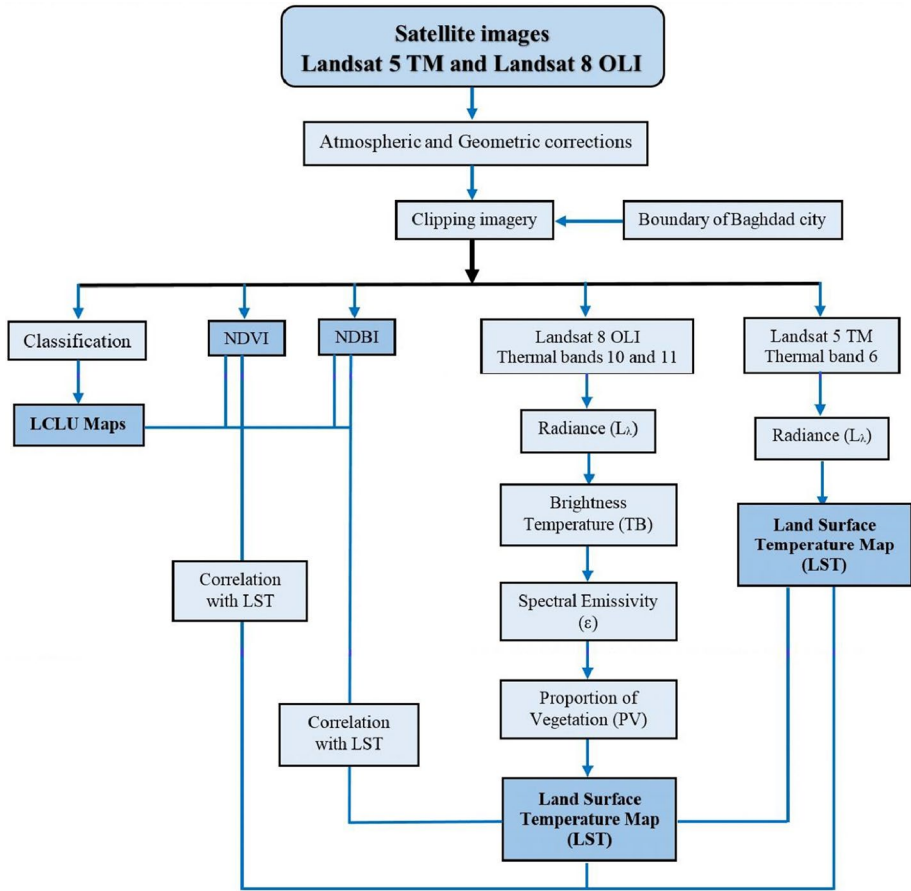
Fig. 2 Flowchart of research methodology used in this study

Table 2 Land cover classification of Baghdad

LULC Types	Description
Water	River, lake/pond, canal, reservoir
Greenland	Orchards, palm groves
Agricultural areas	Wet and dry croplands
Streets and parks	Inner streets and highways, parks, shrubs
Grass areas	Mainly grass field
Residential areas	Commercial areas, urban and rural settlements, industrial areas, public service areas
Barren areas	Sand area, river bank

assessed on accuracy by stratified random sampling method. In this method, the complete study area was divided into small parts; each part is called strata and then samples were randomly chosen from each stratum. The advantage of this method is that the study area

has predefined classes, and when samples are chosen, no class is ignored, whether small or big (Mishra and Pant 2020).

2.3.2 Normalized difference vegetation index calculation

The NDVI was calculated separately for each Landsat image. The NDVI is a commonly used method for monitoring and distinguishing LULC classes. It is a function of the relationship between the Red (R) and Near Infrared (NIR) spectral bands. Therefore, it provides the high and low plant reflectivity in the NIR and R band, respectively, for the visible (VIS) spectrum. The NDVI value ranges from -1 to $+1$, with values from -1 to 0 representing water and other types of surfaces, while values from 0 to $+1$ are for plants. The Normalized Difference Built-Up Index (NDBI) used NIR, Mid IR (MIR) and Shortwave IR (SWIR) bands in Landsat 5 and 8 images for mapping the built-up and bare land in urban area (Zha et al. 2003a, b; Salman et al. 2020). The values of NDBI range from -1 to $+1$. A positive value indicates water bodies and highly built-up areas, while negative values represent other land cover types (Hashim et al. 2021). (Hashim, Sultan, Attyia, Al Maliki and Al-Ansari) (Hashim, Sultan, Attyia, Al Maliki and Al-Ansari) (Hashim, Sultan, Attyia, Al Maliki and Al-Ansari) (Hashim, Sultan, Attyia, Al Maliki and Al-Ansari) [54]Eq. (1) used for NDVI calculation (Hashim et al. 2019a, b):

$$\text{NDVI} = \frac{\text{NIR} - R}{\text{NIR} + R} \tag{1}$$

Equations (1 and 2) were used to calculate NDBI from Landsat 5 and Landsat 8:

$$\text{NDBI (Landsat 5)} = \frac{\text{MIR} - \text{NIR}}{\text{MIR} + \text{NIR}} \tag{2}$$

$$\text{NDBI(Landsat 8)} = \frac{\text{SWIR1} - \text{NIR}}{\text{SWIR1} + \text{NIR}} \tag{3}$$

2.3.3 LST estimation using Landsat images

The normalized surface temperature is prepared using the following steps from thermal band 6 of Landsat 5 TM.

Step 1: Conversion of DN Values to Radiance.

The following Equation is used to convert the digital number (DN) of images to radiance units, expressed as (Ibrahim 2017):

$$L_\lambda = \left(L_{\text{MAX}} - L_{\text{MIN}}\right)/255 \times DN + L_{\text{MIN}\,\lambda} \tag{4}$$

where L_λ: Spectral radiance, L_{MAX}: 15.600 (spectral radiance of DN value 255), L_{MIN}: 1.238 (spectral radiance of DN value 1), DN: Digital Number.

Step 2: Conversion from Radiance (L_λ) to LST in °C.

Equation (5) used for conversion the (L_λ) to at-satellite brightness temperature (T_B):

$$T_B = \frac{K_2}{\ln\left(\frac{K_1}{L_\lambda} + 1\right)} - 273.15 \tag{5}$$

where T_B in °C; K_2: Calibration constant 2 (1260.56); K_1: Calibration constant 1 (607.76).

The LST values are calculated using thermal bands (10 and 11) for Landsat 8 OLI (Feng et al. 2014).

Step 1: Conversion of DN values to Top of Atmosphere Radiance (TOA) is estimated using Eq. (6):

$$L_\lambda = M_L \times Q_{\text{cal}} + A_L \tag{6}$$

where M_L: Factor scale = 0.0003342, Qcal: DN of band 10 and 11, A_L: Added factor = 0.1

Step 2: Conversion to T_B in °C

$$T_B = \frac{K_2}{\ln\left(\frac{K_1}{L_\lambda} + 1\right)} - 273.15 \tag{7}$$

where T_B: at-satellite brightness temperature brightness temperature (°C); K_2: Calibration constants (1321.0789 for band 10, and 480.8883 for band 11); K_1: Calibration constants (774.8853 for band 10, and 1201.1442 for band 11).

Step 3: Conversion from T_B to LST in °C.

The LST values are obtained from brightness temperatures with Eq. (8) (Terfa et al. 2020):

$$\text{LST}(°\text{C}) = \frac{T_B}{\left[1 + \lambda\left(\frac{T_B}{P}\right) \times \ln(\varepsilon)\right]} \tag{8}$$

where: T_B = Brightness Temperature in °C; λ = Wavelength of emitted radiance (10.8 μm), P = hc/k (1.438×10^{-2} mk); h = Planck constant (6.626×10^{-34} J s^{-1}); c = velocity of light (2.998×10^8 ms^{-1}); k = Boltzmann constant (1.38×10^{-23} JK^{-1}); ε: Spectral emissivity value, using Eq. (9) (Hishe et al. 2017):

$$\varepsilon = 0.004 \times PV + 0.986 \tag{9}$$

where PV: Proportion of vegetation, calculated using Eq. (10):

$$PV = \left(\frac{\text{NDVI} - \text{NDVI}_{\text{min}}}{\text{NDVI}_{\text{max}} - \text{NDVI}_{\text{min}}}\right)^2 \tag{10}$$

where NDVI min and NDVI max correspond to the NDVI min and NDVI max values in an image, respectively (Sobrino et al. 2004).

Step 4: Calculation of LST based on the above equations for band 11.

The mean LST of bands 10 and 11 was calculated for Landsat 8 OLI image.

2.3.4 Urban–rural gradient analysis

Urban–rural gradient analysis is one technique for analyzing spatial distributions and temporal variations of environmental variables, for instance, LST and landscape

degradation. Urban–rural gradient analysis was used to analyze the spatiotemporal variation of LST, NDBI and NDVI in Baghdad city's urban–rural gradient Zone. This analysis enables us to assess the spatial pattern of LST, NDVI, and NDBI and understand how they change from urban center to sub-urban/rural parts of Baghdad.

There are many methods available for urban–rural analysis, such as Demographic dynamics, Economic and social indicators, Settlement structure, Distance and Hybrid (Cattivelli et al. 2008). Following (Balew and Korme 2020), this study used the circular ring method for urban–rural gradient analysis, where (i) the city center was identified based on the density of built-up; (ii) circular rings were developed using Multiple Ring Buffer analysis and ten zones were extracted with 2 km interval from the city center up to 20 km; (iii) LST, NDVI and NDBI values were extracted for each zone.

3 Results and analysis

3.1 LULC classification categories in Baghdad

Figure 3 shows the results of the supervised classification of Landsat images. It shows a clear variation in LULC of 1984 and 2020 in Baghdad. The water area in Fig. 3a was about 15.6 km^2, represented by the Tigris River and artificial lakes on the Karkh and Rusafa sides. The area of orchards, agricultural, and grass areas in Baghdad amounted to 42.7 km^2, 41.6 km^2 and 208.5 km^2, respectively, in 1984. The streets and parks covered 39 km^2, the residential area, 227.8 km^2 and barren lands, 315.6 km^2 in 1984. Figure 3b shows that the
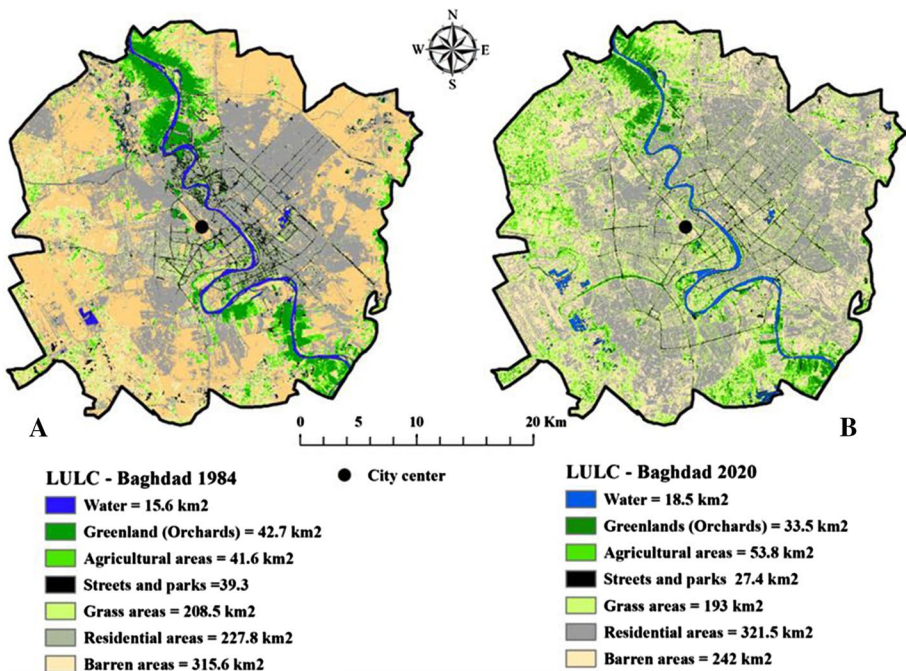

Fig. 3 LULC categories classification in Baghdad; **A** Landsat 5 in 1984, and **B** Landsat 8 in 2020
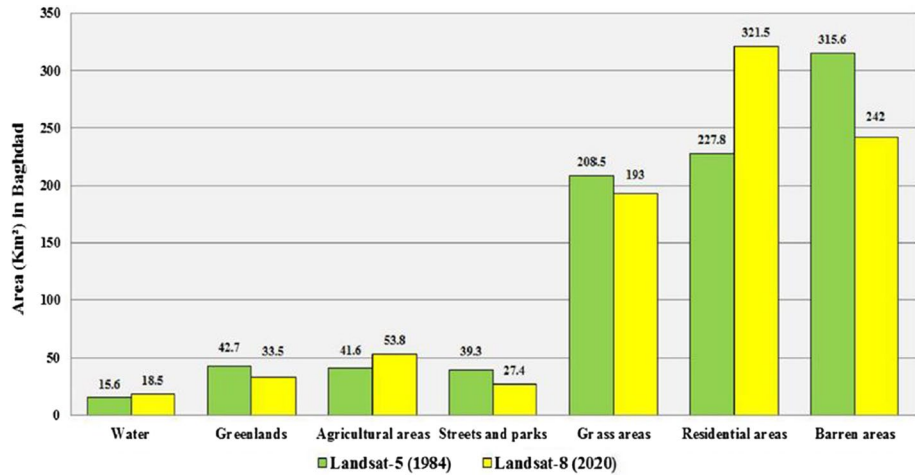
Fig. 4 Comparison of LULC in Baghdad between 1984 and 2020

Table 3 The percentage of the areas under different LULC categories changed between 1984 and 2020

LULC category	Area (km2)		Changes (%) in area
	1984	2020	
Water	15.6	18.5	18.6
Greenland (Orchards)	42.7	33.5	− 21.5
Agricultural areas	41.6	53.8	29.3
Streets and parks	39.3	27.4	− 30.3
Grass areas	208.5	193	− 7.4
Residential areas	227.8	321.5	41
Barren areas	315.6	242	− 23.3

water area increased to 18.5 km^2 in 2020 compared to 15.6 km^2 in 1984. It was due to the excavation of industrial lakes in the west and south of Baghdad. In addition, the area of orchards and grass areas decreased from 193 km^2 in 1984 to 33.5 km^2 in 2020. In contrast, the agricultural area increased to 53.8 km^2 due to the transformation of some barren areas in the west and northwest Baghdad to agricultural areas. The prominent feature of LULC in Baghdad is the increase in the residential areas at the expense of agricultural and barren areas. It was increased to 321.5 km^2 in 2020 compared to 227.8 km^2 in 1984. This explains the decrease in the barren area in 2020 to 242 km^2, compared to 315.6 km^2 in 1984.

Figure 4 shows the comparison of LULC of Baghdad city obtained using Landsat 5 in 1984 and Landsat 8 images in 2020. The decreases in orchards, grass, parks and even barren areas conversely led to increased residential areas during 1984–2020. In contrast, Table 3 shows the percentage of the area changed under different LULC categories in Baghdad during 1984–2020. The great reduction in LULC in Baghdad was in the vegetation area, as the total area of green lands (orchards), streets, parks and grass areas about 75% compared to other types of LULC, between 1984 and 2020. In contrast, the residential areas increased to 41%. It is also noted that the agricultural areas have increased to more than 29.3%, especially in the surrounding areas of Baghdad. The water area also increased
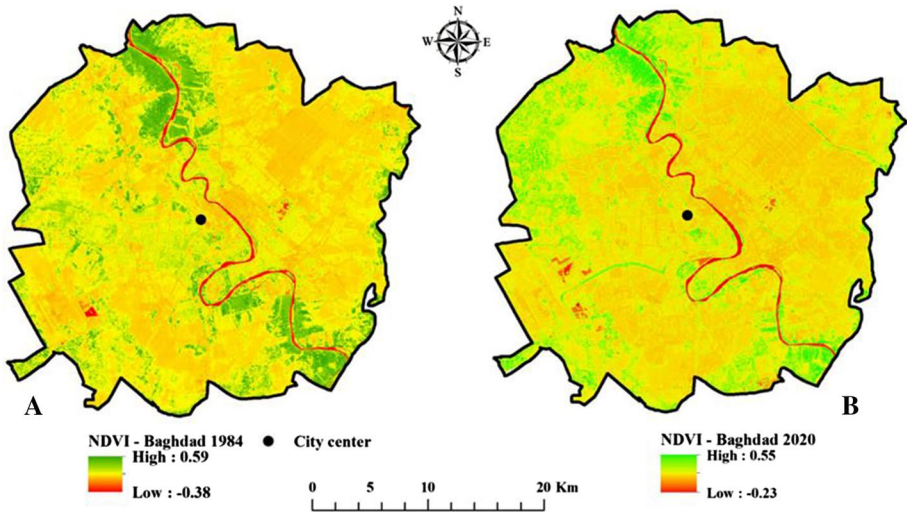
Fig. 5 The NDVI values of Baghdad estimated from **A** Landsat 5 in 1984; and **B** Landsat 8 in 2020

to 18.6%, due to industrial lakes, especially in western and southern Baghdad. In addition, the barren areas decreased to 23.3% due to conversion to residential areas. Increased residential area indicates increasing population and the continuous urban expansion of Baghdad. The results indicate urbanization is the most vital and active force of LULC changes (Hu et al. 2016; Mosammam et al. 2017).

3.2 Normalized difference vegetation index

Figure 5 shows the NDVI values of Baghdad city estimated from Landsat images in the years 1984 and 2020. The scale of NDVI values of Landsat 5 image (Fig. 5a) was in the range of -0.38 and 0.59 in 1984. The areas in northern Baghdad on both sides of the Tigris River in Karkh and Rusafa governorate and Al-Dora and Al-Zafaraniyah in the south of the river were covered by palm orchards and farms, which resulted in extensive vegetation cover, represented by a high NDVI of 0.59. Greenland areas were on the outskirts of Baghdad and the Karkh side in the west of Baghdad due to the lack of urban and residential areas and large agricultural lands.

On the other hand, the eastern side of Baghdad in Rusafa was distinguished by its large residential areas, especially in Al-Sadir City, New Baghdad and Al-Shaab. The NDVI values for Baghdad in 2020 were ranged between -2.23 and 0.55, as shown in Fig. 5b. Many palm orchards scattered on both sides of the Tigris River have shrunk for several reasons, including drought, their transformation into residential or barren areas, and weak governance. These reasons helped the owners of the lands to manipulate and raze them in many cases. This caused a deterioration of the vegetation cover of Baghdad in 2020 and a significant decrease in green areas. On the other hand, non-green areas, such as urban areas, increased due to large urban expansion in Baghdad to accommodate the rising population.
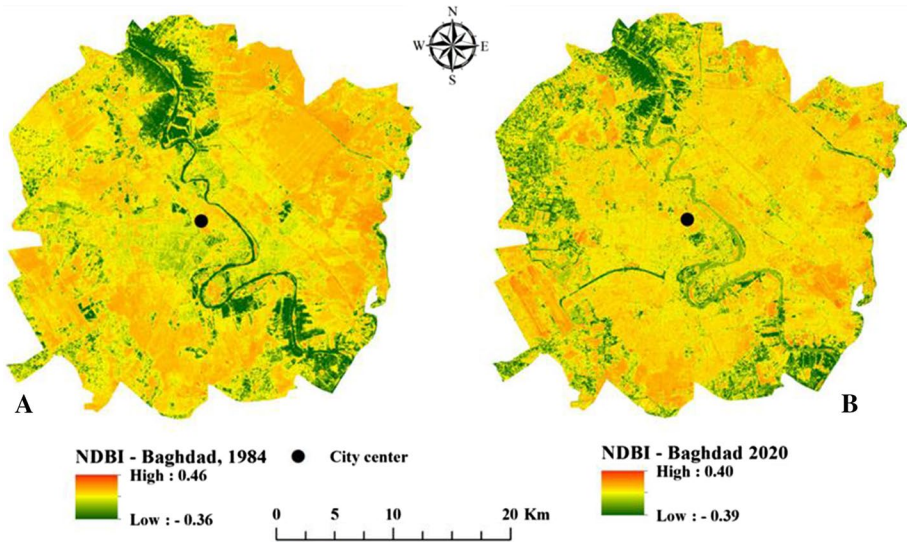
Fig. 6 The NDBI values of Baghdad estimated using **A** Landsat 5 in 1984; and **B** Landsat 8 in 2020

3.3 Normalized difference built-up index

Figure 6 shows the NDBI values for Baghdad city in 1984 and 2020. The figure shows that the minimum value of Landsat 5 image was − 0.36 in 1984. These values recorded along the Tigris River, north and south Baghdad, and some areas in the city center and the western parts of Baghdad. The positive NDBI values demonstrated in the other parts of Baghdad, especially in the Al-Rusafa region.
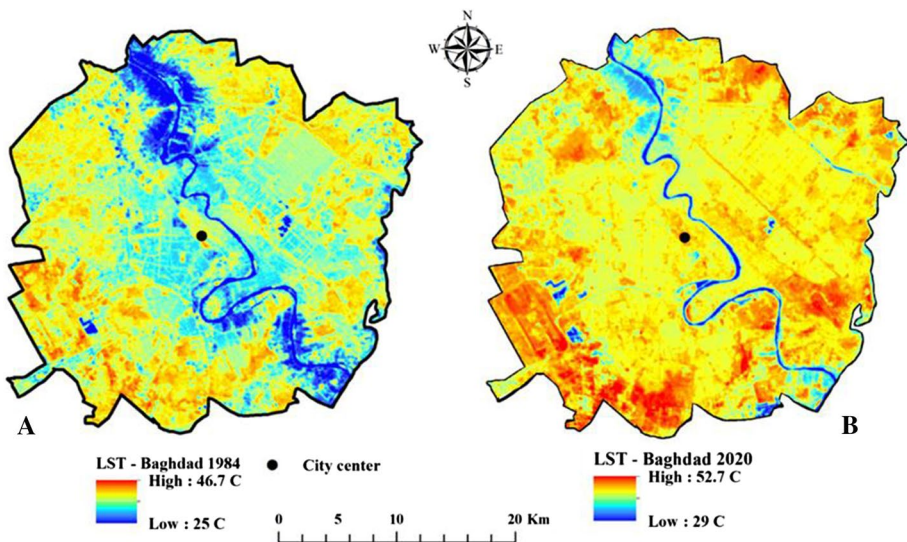
Fig. 7 The LST of Baghdad based on; **A** Landsat 5 in 1984, and **B** Landsat 8 in 2020

In 2020, the NDBI values for Baghdad ranged between −0.39 and 0.40, as shown in Fig. 6b. The LULC maps showed a spread of the suburbs of Baghdad, a large number of informal settlements, especially in agricultural and barren areas. These settlements were concentrated in eastern Baghdad on the Rusafa side, on the outskirts of Al-Sadir and New Baghdad. Besides, informal settlements spread was noticed in the north and south of Karkh, in Al-Kadhimiya and Al-Dora. In Baghdad, the informal settlement sector represents about 3.3 million or 26% of the total housing.

3.4 Land surface temperature of Baghdad

Figure 7 shows the LST extracted from thermal bands of Landsat images, obtained on August 27, 1984, and from Landsat 8 image on August 30, 2020. The LST values ranged between 25 and 46.7 °C in 1984, as shown in Fig. 7a. In contrast, it was ranged from 29 to 52.7 °C in 2020 (Fig. 7b). This large difference (nearly 6 °C) in the LST between 1984 and 2020 explains the evident rise in temperatures in Iraq in recent years. During the same period, the minimum LST increased by nearly 4 °C, as shown in Fig. 7.

The LST also correlated well with the LULC variations in Baghdad. Figure 8 shows that the lowest LST in 1984 was 25 °C, mostly over the green lands (orchards), water, and agricultural lands. It was more than 40 °C in the residential areas spread on both sides of the Tigris River. The highest LST was more than 46 °C in barren areas spread in the outskirts of Baghdad. The LST estimated in Baghdad was significantly different in 2020 relative to the year 1984 due to the change in LULC, which was evident in Fig. 3 and the variation in the values of (NDVI and NDBI) in Figs. 5 and 6, respectively. The lowest LST recorded was 29 °C, over a narrow strip surrounding the Tigris River and some scattered locations in Baghdad.

The LST in the orchard and agricultural areas was 35 °C and 39.7 °C, respectively. The LST in parks and grass areas was higher, 42.5 °C and 44.3 °C, respectively, showing a clear difference from 1984. The residential and barren areas recorded the highest LST in Baghdad in 2020, 46.7 °C and 52.7 °C, respectively. The changes in LULC in Baghdad in 2020 compared to 1984 led to an increase in LST, exceeded 50 °C.
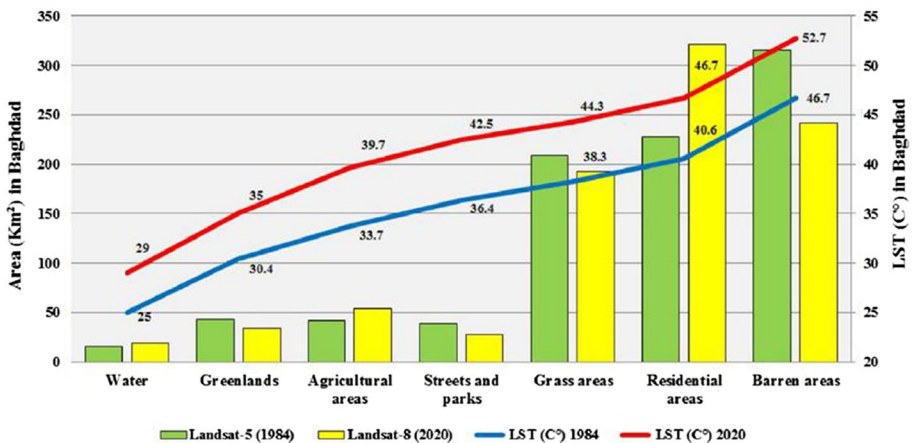

Fig. 8 Correlation between the LST and LULC of Baghdad of 1984 and 2020

The most pronounced observation was the occurrence of a significant UHI of 52 °C in different areas of Baghdad, such as Al-Dora in the vicinity of Al-Dora refinery in the south of Baghdad. There were also UHI in the west and south of Baghdad and northwestern Baghdad in Al-Kadhimiya and Al-Shula, which were among the areas where residential communities and industrial activities are widespread. In Rusafa, the UHI was concentrated in Al-Zafaraniya, southeast of Baghdad, one of the areas inhabited by population and industrial activities.

The high UHI was also noticed in the residential areas or barren lands without vegetation cover on the outskirts of Al-Sadir and Al-Shaab in northeastern Baghdad. The
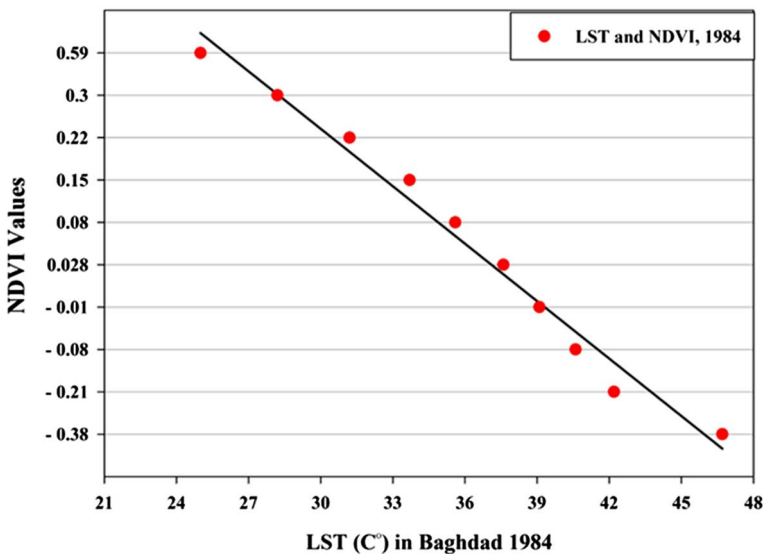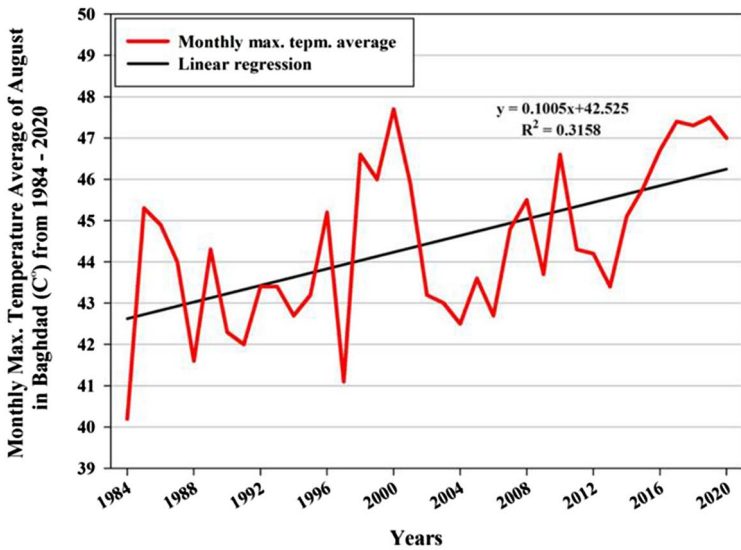

Fig. 9 The monthly maximum temperature average of August in Baghdad during 1984 − 2020

spread of informal areas after 2003 is a major cause of LULC changes and an increase in LST in Baghdad (Hamza 2015). The municipality that suffers most from informal settlements in Baghdad is Al-Ghadeer municipality, followed by the new Baghdad, Al-Kadhimiya and Al-Rusafa. The land surface temperature is governed by physical conditions, i.e., topography, land use and vegetation, of the city/urban areas. The distribution of vegetation, built-up, open land, water bodies and other features determines the surface temperature (Chen et al. 2006).

The above results were broadly consistent with the analysis of August's monthly maximum temperature average in Baghdad for the period 1984 − 2020, based on IMOS
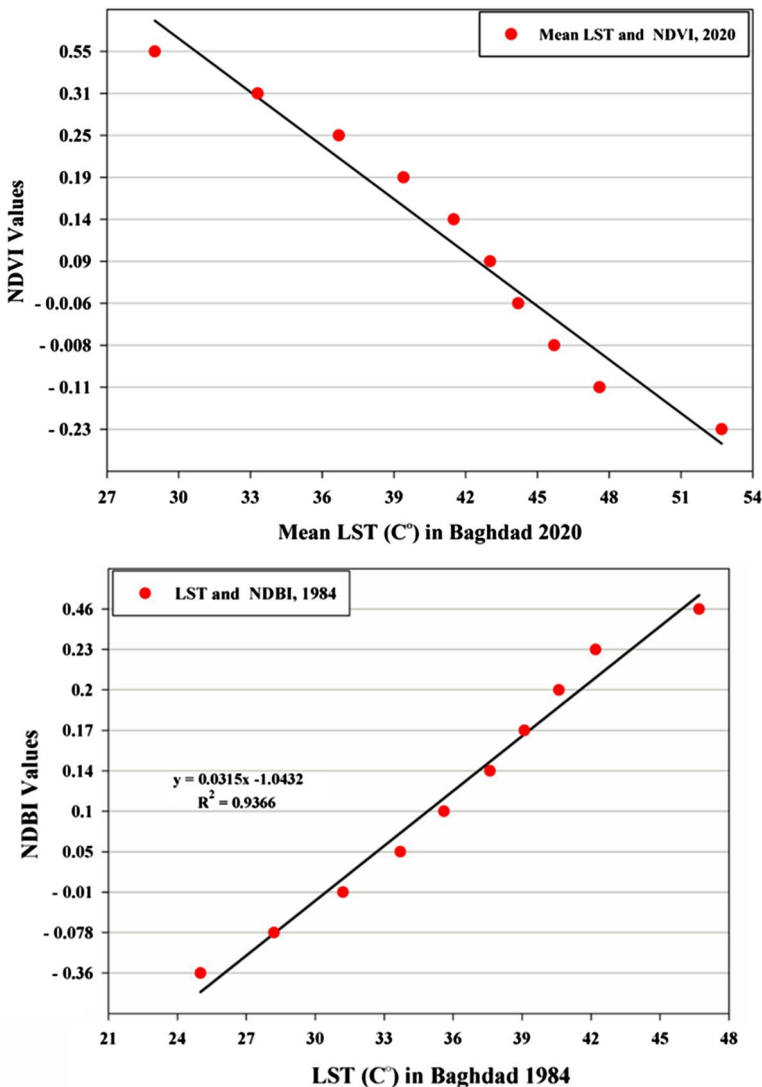

Fig. 10 The relationship between the LST and the NDVI values in 1984 and 2020 for Baghdad
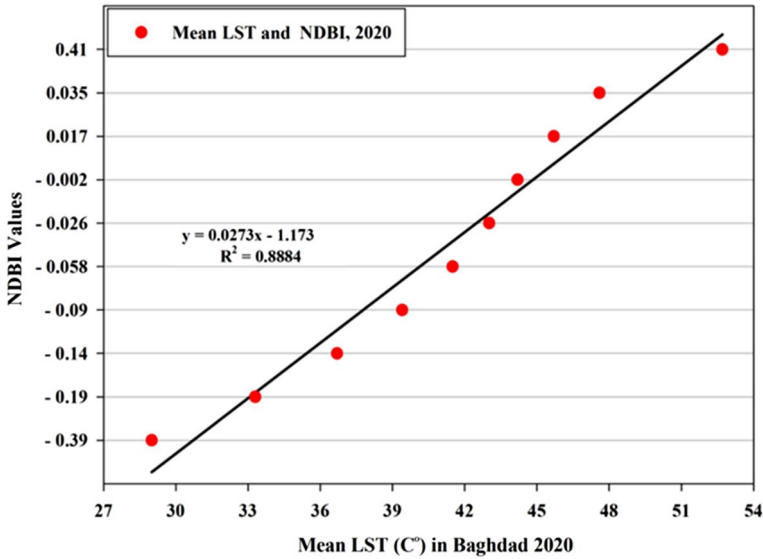
Fig. 11 The relationship between LST and NDBI for Baghdad in 1984 and 2020

data, as shown in Fig. 9. The average maximum temperature in Baghdad in August 1984 was 40.2 °C, while it was 47 °C in August 2020. It indicates an increase of 6.8 °C or 17% during 1984–2020. The results revealed a strong relationship between LST and LULC in 1984 and 2020, which led to a clear rise in temperature in recent years. August's high average maximum temperature also indicates the consequences of climate change. Figure 10 shows the relationship between the LST and NVDI in 1984 and 2020.

Table 4 The mean of LST, NDVI and NDBI at different distances from the city center of Baghdad in 1984 and 2020

| Zone	Distance (km)	1984			2020		
		Mean LST	Mean NDVI	Mean NDBI	Mean LST	Mean NDVI	Mean NDBI
Center	0	39.7	0.01	0.21	45.4	0.06	0.5
Z1	2	37.5	0.03	0.15	43.6	0.09	0.12
Z2	4	36.4	0.02	0.14	42.8	0.07	0.14
Z3	6	36.7	0.026	0.143	42.5	0.073	0.12
Z4	8	36.5	0.026	0.147	42.7	0.08	0.13
Z5	10	37.8	0.027	0.16	43.4	0.051	0.4
Z6	12	38.5	0.033	0.17	42.6	0.1	0.3
Z7	14	39.2	0.031	0.173	44.2	0.08	0.18
Z8	16	37	0.048	0.164	44.4	0.05	0.2
Z9	18	34.4	0.062	0.15	43.5	0.14	0.15
Z10	20	38.8	0.04	0.164	44.2	0.12	0.4
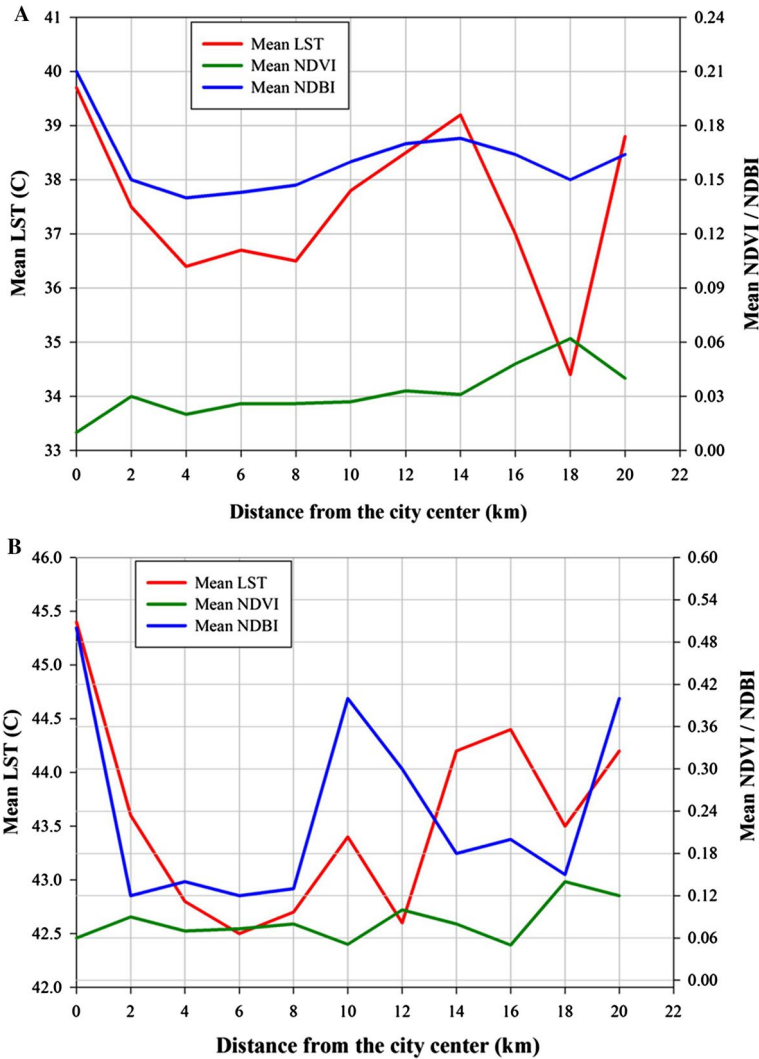
Fig. 12 Urban–rural gradient of LST, NDVI and NDBI in Baghdad in **A** 1984; and **B** 2020

Figure 10 shows an inverse negative correlation between LST and NDVI in 1984, with s correlation coefficient (R^2) of 0.9697. The figure also shows an inverse negative correlation between LST and NDVI in 2020, with $R^2 = 0.9639$.

The correlations between LST and NDBI in 1984 and 2020 are presented in Fig. 11. The results of the linear correlation indicate a positive relationship between LST and NDBI in 1984 and 2020, with $R^2 = 0.9366$ and 0.8884, respectively. The built-up and bare areas showed higher LST values in thermal bands of Landsat 5 and 8 compared to other LULC categories, such as vegetation and water. The literature studies also indicated a positive relationship between residential and bare areas with the thermal signatures of band 6 in Landsat 5 TM and bands 10 and 11 in Landsat 8 OLI (Zha et al. 2003a, b; Ibrahim 2017).

3.5 Analysis of urban–rural gradient

Table 4 and Fig. 12 show the urban–rural gradient of LST, NDVI and NDBI and their spatial pattern for Baghdad in 1984 and 2020. The mean of LST, NDVI and NDBI values at the center of Baghdad in 1984 were 39.7 °C, 0.01 and 0.21, respectively. Those were 37.5 °C, 0.03 and 0.15, respectively 2 km (Z1) away from the center of Baghdad. There was an inverse relationship between LST and NDVI, as shown in Fig. 12a. In contrast, there is a direct relationship between LST and NDBI. LST significantly decreased to 34.4 °C at a distance more than 14 km from the city center, with a mean NDVI and NDBI of 0.062 and 0.15, respectively. Agricultural areas and orchards spread on the northern and southeastern edges of the Tigris River and western parts in Baghdad, which led to a rise in NDVI. Conversely, LST and NDBI decreased accordingly.

The rural areas in 1984 were concentrated along the Tigris River and in western Baghdad. In 2020, LST in the center of Baghdad was 45.4 °C, with a mean NDVI and NDBI of 0.06 and 0.5, respectively (Fig. 12b). LST and NDBI decreased to 43.6 °C and 0.12, and NDVI increased to 0.09 at 2 km away from the city center. The LST and NDBI values increased in the areas between 8–10 km and 18–20 km from the city center due to large urbanization in 2020 at the expense of green and barren areas. The reason was the irregular and often random urban sprawl, especially in areas considered poor, densely populated and located on the outskirts of high-end neighborhoods.

At an 18 km distance from the city center, LST slightly decreased to 43.5 °C, with a mean NDVI of 0.12 and a mean NDBI of 0.15. The green and orchards areas decreased in 2020 after 18 km away from the city center compared to 14 km in 1984. The mean of LST NDBI also rose. In Baghdad, the informal settlement sector represents around 26% of the total housing. The majority of informal settlements are implemented on agricultural or suburban lands. The buildings are constructed either with concrete, blocks, or tin plates (Abouelmagd 2020).

The results showed that the areas surrounding Baghdad, which are mostly barren, have higher temperatures than the urban areas. The heat in the surroundings is directly absorbed by the bare ground, causing it to heat up faster than other covered ground. Besides, roads, sidewalks, buildings, concrete and other features that make up the urban surfaces tend to retain heat for a longer period. The randomly constructed built lands over the lack of green spaces in the outskirts of Baghdad retain heat for a longer period than the other land cover classes.

4 Discussion

Baghdad is Iraq's capital and a major managerial center, and one of the largest urban centers in the middle east. It is also considered Iraq's biggest economic and administrative center, which is almost covered by built-up areas. The Landsat 5 TM and Landsat 8 OLI thermal images were used to retrieve LST in this present study and analyze the spatial pattern of LST and its variation with different LULC types in Baghdad. The results showed that the spatial extent of residential areas of Baghdad increased from 227.8 km^2 in 1984 to 321.5 km^2 in 2020. The urban sprawl in Baghdad extended through the conversion of agricultural and barren areas to meet the housing crisis of increased population and the lack of sustainable city planning to address it.

Table 5 Mean LST difference (℃) from the center of Baghdad in 1984 and 2020

Zone	Distance (km)	Mean LST		Mean LST (Difference)
		1984	2020	1984–2020
Center	0	39.7	45.4	5.7
Z1	2	37.5	43.6	6.1
Z2	4	36.4	42.8	6.4
Z3	6	36.7	42.5	5.8
Z4	8	36.5	42.7	6.2
Z5	10	37.8	43.4	5.6
Z6	12	38.5	42.6	4.1
Z7	14	39.2	44.2	5
Z8	16	37	44.4	7.8
Z9	18	34.4	43.5	9.1
Z10	20	38.8	44.2	5.4

Rural areas in Baghdad suffer from higher levels of deprivation. The more the agglomeration grows bigger, the less deprivation occurs and reaches its lowest levels in large cities (Al shouk et al. 2016). This caused random settlements on both Karkh and Rusafa in Baghdad, affecting LULC and LST in 2020. The results showed that the spatial patterns of LST increased from south and southwest of Baghdad in 1984 toward north, east, southeast in 2020, especially in random settlements. Barren and urban areas recorded the highest LST, 52.7 °C and 46.7 °C, respectively. The LST for barren and urban areas recorded 46.7 °C and 40.6 °C in 1984, respectively. On the other hand, water and green lands categories recorded the lowest LST, at 25 °C and 30.4 °C, in 1984, respectively, and recorded 29 °C and 35 °C, respectively, in 2020. The results illustrated that the spatiotemporal variation of LST has been associated with urban expansion and its LULC alteration, which affected the presence and localization of UHI in Baghdad, especially in the suburbs regions. Some researchers found similar results during their studies in four African cities and Bihar Dar city, respectively (Simwanda et al. 2019; Balew and Korme 2020). The study also evaluated the LST variation in urban–rural gradient zones in 1984 and 2020, as shown in Table 5. At the center of Baghdad, the mean LST increased 5.7 °C in 2020 from 1984. At 2 km and 4 km away from the center of Baghdad, the mean LST increased by 6.1 °C and 6.4 °C, respectively, in 2020 than 1984.

The largest increase in mean LST was recorded at 16 km and 18 km distance from the city center, 7.8 °C and 9.1 °C, respectively. Urban expansion and its associated LULC transformation increased LST and vegetation losses. The expansion of built-up areas has changed the local air quality natural environment (Mustafa and Szydłowski 2020). Besides, high UHI caused negative effects on landscape aesthetics, energy efficiency, human health and quality of living in urban environments (Yue et al. 2007).

5 Conclusion

Baghdad's LST, NDVI and UHI changes during 1984−2020 were evaluated in this study using Landsat images. The LST values were calculated using thermal bands of Landsat 5 TM on August 27, 1984, and Landsat 8 OLI on August 30, 2020. The study area was

classified into seven LULC classes: water, orchards, agricultural areas, streets and parks, grass, residential and barren areas. The results showed an increase in residential areas from 1984 to 2020, about 94 km^2, where a decrease in vegetation areas (orchards, parks and grass areas) by 35.6 km^2. Water bodies and agricultural areas increased by 18.6% and 29.3%, while the grass and barren areas decreased by 7.4% and 23.3%, respectively, during the study period. The study showed a strong relationship between LST and LULC. LST showed large variations for different LULC; for instance, the barren and residential areas exhibited higher radiant temperatures.

The observed higher temperatures in Baghdad's residential and barren areas might negate the previous reports of higher LST values in urbanized areas as found in the existing literature. This led to the UHI effect in the west, south and northwestern of Baghdad and surrounding areas in the east, southeast, and northeast of Baghdad. Higher LST is seen in areas with less vegetated LULC and vice versa. Also, the study found that the average maximum temperature in Baghdad in August 1984 was 40.2 °C, while the temperature for the same month in 2020 was 47 °C. This indicates an increase of 6.8 °C or about 17% between 1984 and 2020. Different land use/land cover classes have different LST, NDVI and NDBI (Yue et al. 2007). Areas with vegetation and water body showed lower temperatures than the built-up areas (Joshi and Bhatt 2012).

The results showed how the unplanned use of the different lands led adversely affects the city environment. This, however, calls for appropriate strategies to reduce the contribution of these factors to global warming and assist in promoting a sustainable economy to face the change. An analysis of urban and rural gradation in Baghdad shows the impact of urban areas in the city center and the surrounding areas. At the same time, the rural regions were spread in the suburbs, especially in the north and south of Baghdad. The results presented in this study would help urban planners and decision-makers for the future planning of Baghdad.

Data availability Data can be provided upon request from the corresponding author.

Declarations

Conflict of interest The authors declare no conflict of interest.

Ethical approval The manuscript is conducted within the ethical manner advised by the NH.

Consent to publish The research is scientifically consented to be published.

References

Abouelmagd SAS (2020) The rehabilitation of slums and informal settlements in greater Cairo: applying a livelihood perspective to evaluate existing policy and implementation approaches

Al Qeisi S (2012) The city of Baghdad between the reality of rapid growth and the relay of master plans and lack of integration of the planning process. 0–17

Alam A, Bhat MS, Maheen M (2020) Using Landsat satellite data for assessing the land use and land cover change in Kashmir valley. GeoJournal 85:1529–1543

Al-Shammari MMA, Al-Shammaa AM, Al Maliki A et al (2021) Integrated water harvesting and aquifer recharge evaluation methodology based on remote sensing and geographical information system: case study in Iraq. Nat Resour Res. https://doi.org/10.1007/s11053-021-09835-3

Ayanlade A (2016) Seasonality in the daytime and night-time intensity of land surface temperature in a tropical city area. Sci Total Environ 557–558:415–424. https://doi.org/10.1016/j.scitotenv.2016.03.027

Balew A, Korme T (2020) Monitoring land surface temperature in Bahir Dar city and its surrounding using Landsat images. Egypt J Remote Sens Sp Sci. https://doi.org/10.1016/j.ejrs.2020.02.001

Bao T, Li X, Zhang J et al (2016) Assessing the distribution of urban green spaces and its anisotropic cooling distance on urban heat island pattern in Baotou, China. ISPRS Int J Geo-Inf 5:12. https://doi.org/10.3390/ijgi5020012

Beyaztas U, Salih SQ, Chau K-W et al (2019) Construction of functional data analysis modeling strategy for global solar radiation prediction: application of cross-station paradigm. Eng Appl Comput Fluid Mech 13:1165–1181

Buyantuyev A, Wu J (2009) Urban heat islands and landscape heterogeneity: linking spatiotemporal variations in surface temperatures to land-cover and socioeconomic patterns. Landsc Ecol 25:17–33. https://doi.org/10.1007/s10980-009-9402-4

Cai G, Du M, Xue Y (2011) Monitoring of urban heat island effect in Beijing combining ASTER and TM data. Int J Remote Sens 32:1213–1232. https://doi.org/10.1080/01431160903469079

Calice C, Clemente C, Salvati A et al (2017) Urban heat island effect on the energy consumption of institutional buildings in rome. IOP Conf Ser Mater Sci Eng 245:82015. https://doi.org/10.1088/1757-899x/245/8/082015

Cattivelli L, Rizza F, Badeck FW et al (2008) Drought tolerance improvement in crop plants: an integrated view from breeding to genomics. F Crop Res 105:1–14. https://doi.org/10.1016/j.fcr.2007.07.004

Chen X-L, Zhao H-M, Li P-X, Yin Z-Y (2006) Remote sensing image-based analysis of the relationship between urban heat island and land use/cover changes. Remote Sens Environ 104:133–146. https://doi.org/10.1016/j.rse.2005.11.016

Erasu D (2017) Remote sensing-based urban land use/land cover change detection and monitoring. J Remote Sens GIS 6:5

Fan C, Myint S, Kaplan S et al (2017) Understanding the impact of urbanization on surface urban heat islands—a longitudinal analysis of the oasis effect in subtropical desert cities. Remote Sens 9:672. https://doi.org/10.3390/rs9070672

Faqe Ibrahim G (2017) Urban land use land cover changes and their effect on land surface temperature: case study using Dohuk city in the Kurdistan region of Iraq. Climate 5:13. https://doi.org/10.3390/cli5010013

Faroughi M, Karimimoshaver M, Aram F et al (2020) Computational modeling of land surface temperature using remote sensing data to investigate the spatial arrangement of buildings and energy consumption relationship. Eng Appl Comput Fluid Mech 14:254–270

Feng H, Zhao X, Chen F, Wu L (2014) Using land use change trajectories to quantify the effects of urbanization on urban heat island. Adv Sp Res 53:463–473. https://doi.org/10.1016/j.asr.2013.11.028

Feng Y, Li H, Tong X et al (2018) Projection of land surface temperature considering the effects of future land change in the Taihu Lake Basin of China. Glob Planet Change. https://doi.org/10.1016/j.gloplacha.2018.05.007

Fu P, Weng Q (2016) A time series analysis of urbanization induced land use and land cover change and its impact on land surface temperature with Landsat imagery. Remote Sens Environ 175:205–214. https://doi.org/10.1016/j.rse.2015.12.040

Gajić A, Krunić N, Protić B (2021) Classification of rural areas in serbia: framework and implications for spatial planning. Sustainability 13:1596. https://doi.org/10.3390/su13041596

Hahs AK, McDonnell MJ (2006) Selecting independent measures to quantify Melbourne's urban–rural gradient. Landsc Urban Plan 78:435–448

Hamza SM (2015) Slums in Baghdad city: Analytical planning study

Hashim BM, Sultan MA, Attyia MN, Al Maliki AA, Al-Ansari N (2019a) Change detection and impact of climate changes to Iraqi southern marshes using landsat 2 MSS, landsat 8 OLI and sentinel 2 MSI data and GIS applications. Appl Sci. https://doi.org/10.3390/app9102016

Hashim BM, Sultan MA, Attyia MN et al (2019b) Change detection and impact of climate changes to Iraqi southern marshes using landsat 2 MSS, landsat 8 OLI and sentinel 2 MSI data and GIS applications. Appl Sci 9:2016. https://doi.org/10.3390/app9102016

Hashim BM, Al-Naseri SK, Al-Maliki A, Al-Ansari N (2020) Impact of COVID-19 lockdown on NO2, O3, PM2.5 and PM10 concentrations and assessing air quality changes in Baghdad, Iraq. Sci Total Environ 754:141978. https://doi.org/10.1016/j.scitotenv.2020.141978

Hashim BM, Al-Naseri SK, Al-Maliki A, Al-Ansari N (2021) Impact of COVID-19 lockdown on NO2, O3, PM2.5 and PM10 concentrations and assessing air quality changes in Baghdad, Iraq. Sci Total Environ 754:141978. https://doi.org/10.1016/j.scitotenv.2020.141978

Hishe S, Lyimo J, Bewket W (2017) Effects of soil and water conservation on vegetation cover: a remote sensing based study in the Middle Suluh River Basin, northern Ethiopia. Environ Syst Res. https://doi.org/10.1186/s40068-017-0103-8

Hu Y, Jia G, Pohl C et al (2016) Assessing surface albedo change and its induced radiation budget under rapid urbanization with Landsat and GLASS data. Theor Appl Climatol. https://doi.org/10.1007/s00704-015-1385-2

Hussain A, Bhalla P, Palria S (2014) Remote sensing based analysis of the role of land use/land cover on surface temperature and temporal changes in temperature; a case study of Ajmer District, Rajasthan. ISPRS Int Arch Photogramm Remote Sens Spat Inf Sci XL–8:1447–1454

Jassim HM, Ibraheem FH, Zangana BFA (2014) Environmental issues caused by the increasing number of vehicles in Iraq. Energy Sustain. V

Joshi JP, Bhatt B (2012) Estimating temporal land surface temperature using remote sensing: a study of Vadodara urban area, Gujarat. Int J Geol Earth Environ Sci 2:123–130

Karimi Firozjaei M, Fathololoumi S, Kiavarz M et al (2021) Land surface ecological status composition index (LSESCI): a novel remote sensing-based technique for modeling land surface ecological status. Ecol Indic 123:107375. https://doi.org/10.1016/j.ecolind.2021.107375

Kemarau RA, Eboy OV (2020) Urbanization and it impacts to land surface temperature on small medium size city for year 1991, 2011 and 2018: case study Kota Kinabalu. J Borneo Soc Transform Stud 6:58–76. https://doi.org/10.51200/jobsts.v6i1.2791

Khan N, Shahid S, Sharafati A et al (2021) Determination of cotton and wheat yield using the standard precipitation evaporation index in Pakistan. Arab J Geosci 14:1–16

Kumar KS, Bhaskar PU, Padmakumari K (2012) Estimation of land surface temperature to study urban heat island effect using landsat Etm+ Image. Int J Eng Sci Technol

Kumar D, Shekhar S (2015) Statistical analysis of land surface temperature–vegetation indexes relationship through thermal remote sensing. Ecotoxicol Environ Saf 121:39–44. https://doi.org/10.1016/j.ecoenv.2015.07.004

Li M, Zang S, Zhang B et al (2014) A review of remote sensing image classification techniques: the role of spatio-contextual information. Eur J Remote Sens 47:389–411. https://doi.org/10.5721/eujrs20144723

Lo CP, Quattrochi DA (2003) Land-use and land-cover change, urban heat island phenomenon, and health implications. Photogramm Eng Remote Sens 69:1053–1063. https://doi.org/10.14358/pers.69.9.1053

Lu D, Weng Q (2007) A survey of image classification methods and techniques for improving classification performance. Int J Remote Sens 28:823–870. https://doi.org/10.1080/01431160600746456

Lv Z, Zhou Q (2011) Utility of landsat image in the study of land cover and land surface temperature change. Procedia Environ Sci 10:1287–1292. https://doi.org/10.1016/j.proenv.2011.09.206

Mallick J, Rahman A, Singh CK (2013) Modeling urban heat islands in heterogeneous land surface and its correlation with impervious surface area by using night-time ASTER satellite data in highly urbanizing city, Delhi-India. Adv Sp Res 52:639–655. https://doi.org/10.1016/j.asr.2013.04.025

Masek JG, Wulder MA, Markham B et al (2020) Landsat 9: empowering open science and applications through continuity. Remote Sens Environ 248:111968

McDonnell MJ, Pickett STA (1990) Ecosystem structure and function along urban-rural gradients: an unexploited opportunity for ecology. Ecology 71:1232–1237

Mishra VK, Pant T (2020) Impact of Cluster Sampling on the Classification of Landsat 8 Remote Sensing Imagery. Mach. Intell. Signal Process. 371–381

Mosammam HM, Nia JT, Khani H et al (2017) Monitoring land use change and measuring urban sprawl based on its spatial forms: the case of Qom city. Egypt J Remote Sens Sp Sci. https://doi.org/10.1016/j.ejrs.2016.08.002

Mustafa A, Szydłowski M (2020) The impact of spatiotemporal changes in land development (1984–2019) on the increase in the runoff coefficient in Erbil, Kurdistan Region of Iraq. Remote Sens 12:1302

Oleiwi S, Jalal S, Hamed S et al (2018) Precipitation pattern modeling using cross-station perception: regional investigation. Environ Earth Sci. https://doi.org/10.1007/s12665-018-7898-0

Pour SH, Wahab AKA, Shahid S et al (2020) Low impact development techniques to mitigate the impacts of climate-change-induced urban floods: current trends, issues and challenges. Sustain Cities Soc 62:102373. https://doi.org/10.1016/j.scs.2020.102373

Prakash S, Norouzi H (2020) Land surface temperature variability across India: a remote sensing satellite perspective. Theor Appl Climatol 139:773–784

Rahman A, Kumar S, Fazal S, Siddiqui MA (2012) Assessment of Land use/land cover change in the north-west district of Delhi using remote sensing and GIS techniques. J Indian Soc Remote Sens 40:689–697. https://doi.org/10.1007/s12524-011-0165-4

Salih SQ, Sharafati A, Ebtehaj I et al (2020) Integrative stochastic model standardization with genetic algorithm for rainfall pattern forecasting in tropical and semi-arid environments. Hydrol Sci J. https://doi.org/10.1080/02626667.2020.1734813

Salman SA, Shahid S, Afan HA et al (2020) Changes in climatic water availability and crop water demand for Iraq region. Sustainability 12:3437

Salman SA, Shahid S, Sharafati A et al (2021) Projection of agricultural water stress for climate change scenarios: a regional case study of Iraq. Agriculture 11:1288

Sanikhani H, Deo RC, Samui P et al (2018) Survey of different data-intelligent modeling strategies for forecasting air temperature using geographic information as model predictors. Comput Electron Agric 152:242–260

Sarsam SI, Khafaji HAL (2019) Assessing traffic safety culture among public transport driver population in Baghdad. Indian J Eng 16:80–92

Shalaby A, Tateishi R (2007) Remote sensing and GIS for mapping and monitoring land cover and land-use changes in the Northwestern coastal zone of Egypt. Appl Geogr 27:28–41

Simwanda M, Ranagalage M, Estoque RC, Murayama Y (2019) Spatial analysis of surface urban heat islands in four rapidly growing African cities. Remote Sens 11:1645

Singh R, Grover A, Zhan J (2014) Inter-seasonal variations of surface temperature in the urbanized environment of Delhi using landsat thermal data. Energies 7:1811–1828. https://doi.org/10.3390/en7031811

Sobrino JA, Jiménez-Muñoz JC, Paolini L (2004) Land surface temperature retrieval from LANDSAT TM 5. Remote Sens Environ 90:434–440. https://doi.org/10.1016/j.rse.2004.02.003

Stathopoulou M, Cartalis C (2007) Daytime urban heat islands from Landsat ETM+ and Corine land cover data: An application to major cities in Greece. Sol Energy 81:358–368. https://doi.org/10.1016/j.solener.2006.06.014

Sun C, Wu Z, Lv Z et al (2013) Quantifying different types of urban growth and the change dynamic in Guangzhou using multi-temporal remote sensing data. Int J Appl Earth Obs Geoinf 21:409–417

Terfa BK, Chen N, Zhang X, Niyogi D (2020) Spatial configuration and extent explains the urban heat mitigation potential due to green spaces: analysis over Addis Ababa. Ethiopia Remote Sens 12:2876. https://doi.org/10.3390/rs12182876

Tran H, Uchihama D, Ochi S, Yasuoka Y (2006) Assessment with satellite data of the urban heat island effects in Asian mega cities. Int J Appl Earth Obs Geoinf 8:34–48. https://doi.org/10.1016/j.jag.2005.05.003

Uddin MA, Kamal ASMM, Shahid S (2021) Vegetation Response to Climate and Climatic Extremes in Northwest Bangladesh: A Quantile Regression Approach

Wadduwage S, Millington A, Crossman ND, Sandhu H (2017) Agricultural land fragmentation at urban fringes: an application of urban-to-rural gradient analysis in Adelaide. Land 6:28

Yaseen ZM, Al-Juboori AM, Beyaztas U et al (2019) Prediction of evaporation in arid and semi-arid regions: a comparative study using different machine learning models. Eng Appl Comput Fluid Mech 14:70–89

Yue W, Xu J, Tan W, Xu L (2007) The relationship between land surface temperature and NDVI with remote sensing: application to Shanghai Landsat 7 ETM+ data. Int J Remote Sens 28:3205–3226

Zha Y, Gao J, Ni S (2003b) Use of normalized difference built-up index in automatically mapping urban areas from TM imagery. Int J Remote Sens 24:583–594. https://doi.org/10.1080/01431160304987

Zha Y, Gao J and NI S (2003) Use of normalized difference built-up index in automatically mapping urban areas from TM imagery

Zhu GB, Liu XL, Jia ZG (2006) A multi-resolution hierarchy classification study compared with conservative methods. ISPRS WG II/3, II/6 Workshop Multiple representation and interoperability of spatial data. Hanover, Germany, pp 22–24

Publisher's Note Springer Nature remains neutral with regard to jurisdictional claims in published maps and institutional affiliations.